Mice lacking doublecortin and doublecortin-like kinase 2 display altered hippocampal neuronal maturation and spontaneous seizures

Géraldine Kerjan[a], Hiroyuki Koizumi[a], Edward B. Han[b], Celine M. Dubé[c], Stevan N. Djakovic[d], Gentry N. Patrick[d], Tallie Z. Baram[c], Stephen F. Heinemann[b], and Joseph G. Gleeson[a,1]

[a]Neurogenetics Laboratory, Howard Hughes Medical Institute, Department of Neurosciences, and [d]Department of Neurobiology, University of California at San Diego, La Jolla, CA 92093; [b]Molecular Neurobiology Laboratory, The Salk Institute, La Jolla, CA 92037; and [c]Departments of Anatomy and Neurobiology and Pediatrics, University of California, Irvine, CA 92697

Contributed by Stephen F. Heinemann, February 3, 2009 (sent for review July 24, 2008)

Mutations in doublecortin (*DCX*) are associated with intractable epilepsy in humans, due to a severe disorganization of the neocortex and hippocampus known as classical lissencephaly. However, the basis of the epilepsy in lissencephaly remains unclear. To address potential functional redundancy with murin *Dcx*, we targeted one of the closest homologues, doublecortin-like kinase 2 (*Dclk2*). Here, we report that *Dcx*; *Dclk2*-null mice display frequent spontaneous seizures that originate in the hippocampus, with most animals dying in the first few months of life. Elevated hippocampal expression of c-fos and loss of somatostatin-positive interneurons were identified, both known to correlate with epilepsy. *Dcx* and *Dclk2* are coexpressed in developing hippocampus, and, in their absence, there is dosage-dependent disrupted hippocampal lamination associated with a cell-autonomous simplification of pyramidal dendritic arborizations leading to reduced inhibitory synaptic tone. These data suggest that hippocampal dysmaturation and insufficient receptive field for inhibitory input may underlie the epilepsy in lissencephaly, and suggest potential therapeutic strategies for controlling epilepsy in these patients.

epilepsy | receptive field | pyramidal neuron | dendrites | delamination

Approximately 1 in 10 people will have a seizure sometime during their life, and the prevalence of epilepsy in the general population is ≈3%. Cortical dysplasia, which includes defects in both neocortex and hippocampus, can result from disordered neuronal cell proliferation, migration, or differentiation, and is identified in >25% of children with intractable epilepsy (1), the type of epilepsy associated with the highest morbidity and mortality.

Classical lissencephaly (defined as smooth brain, with simplified or absent gyri and sulci) is due to alterations in neuronal migration and differentiation. The frequency of epilepsy in lissencephaly is probably 100%, and is typically associated with lethality in the first or second decade of life. One of the major causative genes in humans is doublecortin (*DCX*), which encodes a microtubule binding and stabilizing protein (2).

DCX has 2 close homologues in mice, doublecortin-like kinase 1 (*Dclk1*, also known as *Dcamkl1*) and doublecortin-like kinase 2 (*Dclk2*, also known as *Dck2*), both with broad nervous system expression, to include both mitotic neuroblasts and adult neurons, whereas *Dcx* is mostly expressed in postmitotic immature neurons, and also transiently in adult neuroblasts (3). Previous analysis of *Dcx*; *Dclk1* double knockouts demonstrated functional redundancy during cortical and hippocampal lamination (4, 5). To further uncover functional redundancy in the *DCX* gene family, we targeted *Dclk2*, a gene encoding a highly conserved N-terminal doublecortin domain and a C-terminal kinase domain-containing protein (6). Here, we report that mice deficient in both *Dcx* and *Dclk2* display frequent and spontaneous epileptic seizures, bearing some resemblance to the phenotype observed in humans.

Results

***Dclk2* Knockout Leaves *Dcx* and *Dclk1* Expression Intact.** We targeted the gene in murine embryonic stem cells by using a conditional approach (Fig. S1 and Fig. S2*A*) to avoid potential embryonic lethality. We found that *Dclk2* +/− and −/− mice were viable, fertile, and observed at Mendelian ratios throughout life. Careful histological analysis showed normal brain morphology, cortical lamination, and commissure formation. There was no compensatory alteration in expression of the product of either *Dcx* or *Dclk1* (or its alternative splice isoform *Dcl*) in *Dclk2* +/− or −/− mice at either time point tested (Fig. S2 *B* and *C*). Also, immunostaining performed on postnatal day (P)0 wild-type and *Dclk2* −/− sections revealed no appreciable DCX or DCLK1 intensity differences (Fig. S2*D*). We conclude that the absence of *Dclk2* does not induce compensatory changes in expression in any of these known doublecortin family members.

***Dcx*; *Dclk2* Nulls Are Born in Mendelian Ratio but Infrequently Survive Past Weaning.** To test for functional redundancy with other doublecortin family members, we crossed the *Dclk2* knockout to *Dcx* knockout mice. *Dcx* −/*y*; *Dclk2* −/− and *Dcx* −/−; *Dclk2* −/− mice (here referred to as *Dcx*; *Dclk2* nulls) were born in Mendelian ratios but rarely survived to adulthood. Postmortem analysis showed no obvious causes of death. We quantified survival of the *Dcx*; *Dclk2* nulls that were genotyped at 1 week of age and tracked over the subsequent 12 months. Half of the *Dcx*; *Dclk2* nulls used for this assessment survived by the time of weaning (Fig. 1*A*), and only <10% survived past 5 months of age, compared with >95% survival of wild-type littermates.

***Dcx*; *Dclk2* Nulls Display Spontaneous Hippocampal-Onset Seizures.** During the assessment of the cause of death in the *Dcx*; *Dclk2* nulls, we observed that many *Dcx*; *Dclk2* nulls exhibited spontaneous seizures, often associated with behavioral arrest and forelimb myoclonus. These seizures were noted to start at ≈3 weeks of age and were never observed before P16. To determine the focus of the seizures, we performed awake ambulatory EEG recording from 5-week-old surviving *Dcx*; *Dclk2* null and littermate control (*Dcx* +/*y*; *Dclk2* +/−) male mice for 6 h ($n = 2$ each), using stereotaxically implanted electrodes in hippocampal CA1 and dorsal neocortex, and later checked placement histologically (Fig. 1 *B–D*). Three spontaneous epileptic seizures were captured in *Dcx*; *Dclk2* nulls during the recording period, whereas none occurred in

Author contributions: G.K., H.K., E.B.H., C.M.D., T.Z.B., S.F.H., and J.G.G. designed research; G.K., H.K., E.B.H., and C.M.D. performed research; H.K., S.N.D., G.N.P., and T.Z.B. contributed new reagents/analytic tools; G.K., H.K., E.B.H., C.M.D., S.F.H., and J.G.G. analyzed data; and G.K., H.K., and J.G.G. wrote the paper.

The authors declare no conflict of interest.

[1]To whom correspondence should be addressed. E-mail: jogleeson@ucsd.edu.

This article contains supporting information online at www.pnas.org/cgi/content/full/0812687106/DCSupplemental.

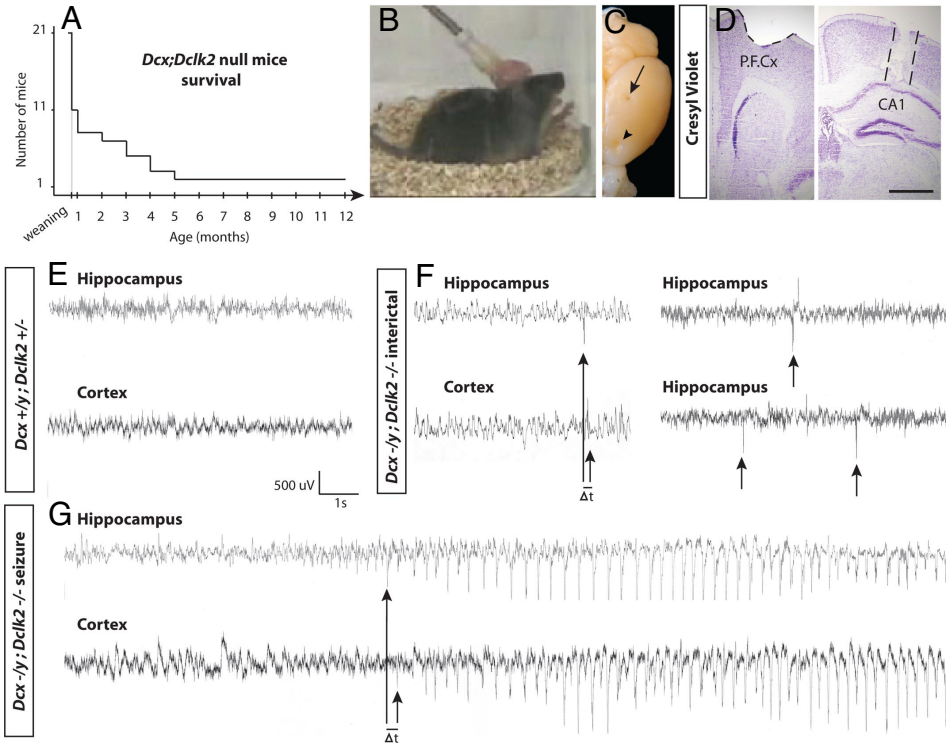

Fig. 1. *Dcx* −/*y*; *Dclk2* −/− mice display spontaneous seizures originating in the hippocampus. (*A*) Kaplan–Meier survival curve for *Dcx*; *Dclk2* nulls. Ten of the 21 died by weaning (3 weeks of age), and 19 died before 5 months of age. (*B*) *Dcx*; *Dclk2* null showing forelimb myoclonus and head retropulsion during awake EEG monitoring. (*C* and *D*) Electrodes implanted under stereotaxis in CA1 (arrow) and frontoparietal cortex (P.F.Cx, arrowhead), validated after recording (*D*). (*E–G*) Concurrent hippocampal and cortical recording in 5-week *Dcx*; *Dclk2* null and littermate. Control shows low amplitude baselines. (*F*) During the interictal period, *Dcx*; *Dclk2* nulls show frequent independent hippocampal spikes (arrows). Rare interictal spikes were also observed in cortex, always preceded by a hippocampal peak (Δ*t*). (*G*) Typical spontaneous electrographic seizure, with onset of epileptiform discharge from hippocampus, with secondary generalization to cortex.

controls (Movie S1). We next examined the interictal EEG recording from *Dcx*; *Dclk2* nulls, commonly used to localize the epilepsy focus. The background activity was punctuated by spontaneous spike (amplitude >2× basal, duration <50 ms) or spike and wave activity, which predominantly originated in the hippocampus. Approximately half of these hippocampal spikes (12 of 22 recorded) were transmitted to the cortex with a Δ*t* of ≈100–250 ms but were not associated with outward changes in behavior (Fig. 1 *E* and *F*). The frequent interictal independent hippocampal discharges suggest a hippocampal focus for the epilepsy in *Dcx*; *Dclk2* nulls.

Before the convulsive attacks, we observed repetitive epileptiform discharges from the hippocampus consisting of 4-Hz monomorphic spike activity. At the onset of the convulsive attack, this activity increased from 400 μV up to 1 mV, and it transitioned into spike and wave appearance at 3-Hz frequency (Fig. 1*G*). Strikingly, the epileptic activity spread to the cortex with a Δ*t* of ≈250 ms, after which the cortex was driving at the same frequency and amplitude as the hippocampus. We conclude that *Dcx*; *Dclk2* nulls display hippocampal-onset epileptic seizures with secondary generalization to tonic–clonic convulsions.

***Dcx; Dclk2* Null Hippocampus Is Strongly Delaminated.** Because the EEG recordings designated the hippocampus as the primary focus of the seizures, we performed a detailed histological study of adult hippocampus organization. *Dcx*; *Dclk2* nulls showed dyslaminated CA3 region, with a small percentage of neurons heterotopically located in the stratum oriens (Fig. 2 *A* and *B*; also found in the *Dcx* −/− as previously reported; see ref. 8). However, *Dcx*; *Dclk2* nulls also showed a discontinuous CA1 field, with a displacement of ≈40% of the neurons to the stratum oriens. We also found reduced packing density of the dentate granule neuron layer, resulting in an increased thickness (Fig. 2 *A* and *B* and Fig. S3*A*), without alteration of the granule cell number per linear millimeter of granule cell layer (GCL). In contrast, we found no apparent defects in organization of the neocortex in *Dcx*; *Dclk2* nulls. We conclude that *Dcx*; *Dclk2* nulls have a compounded dyslamination of the hippocampus.

Increased c-fos Reactivity and Loss of Somatostatin-Positive (SOM+) Interneurons in *Dcx; Dclk2* Nulls. We tested whether *Dcx*; *Dclk2* nulls displayed secondary markers of epilepsy, which have been reported to include elevated *c-fos* expression (9), and loss of somatostatin positive interneurons. At a time after seizure onset (P18), we found a dramatic increase of *c-fos* level in neurons within the stratum pyramidalis, as well as the heterotopic neurons, both the CA2/3 and the CA1 fields (Fig. 2 *C–F*). This finding suggests increased excitability of this class of neurons within the hippocampus, and is consistent with an epileptic phenotype in *Dcx*; *Dclk2* nulls.

The SOM+ hippocampal interneurons are selectively vulnerable to cell death in models of experimental epilepsy (10). At P18, we found ≈50% loss of SOM+ cells in the stratum oriens, as well as other fields in the *Dcx*; *Dclk2* null hippocampus (Fig. 2 *G–I*) compared with controls. This reduction was not due to a loss in overall SOM expression, because the remaining O-LM cells showed normal levels of SOM. They also showed no notable defects in morphology or orientation (Fig. 2 *G* and *H*). No effect on other interneuron subtype numbers such as parvalbumin-positive (Parv+) or calbindin-positive (CaBP+) cells was observed (Fig. 2*J*). This loss of SOM+ cells suggests the possibility of reduced critical inhibitory tone, required to balance the excitatory input on pyramidal neuron dendrites.

Coexpression of *Dcx* and *Dclk2* in Developing Hippocampal Neurons. The dyslaminated CA field suggests a requirement for *Dcx* and *Dclk2* during hippocampal development. Therefore, to identify regions that coexpress *Dcx* and *Dclk2*, we performed in situ hybridizations at embryonic day (E)17, P0, and P6, representing the critical window of hippocampal lamination and development. *Dcx* and *Dclk2* shared the highest levels of expression in the pyramidal neuronal layer of the developing hippocampus at all ages tested (Fig. 3 *A* and *B*). Also, both *Dcx* and *Dclk2* were expressed in the developing dentate GCL and in nonprincipal cell layers containing interneurons.

Lamination of Hippocampal Excitatory Neurons Before the Onset of Epilepsy. To identify the origin of epilepsy, we examine the hippocampus at a time before seizure onset but after the completion

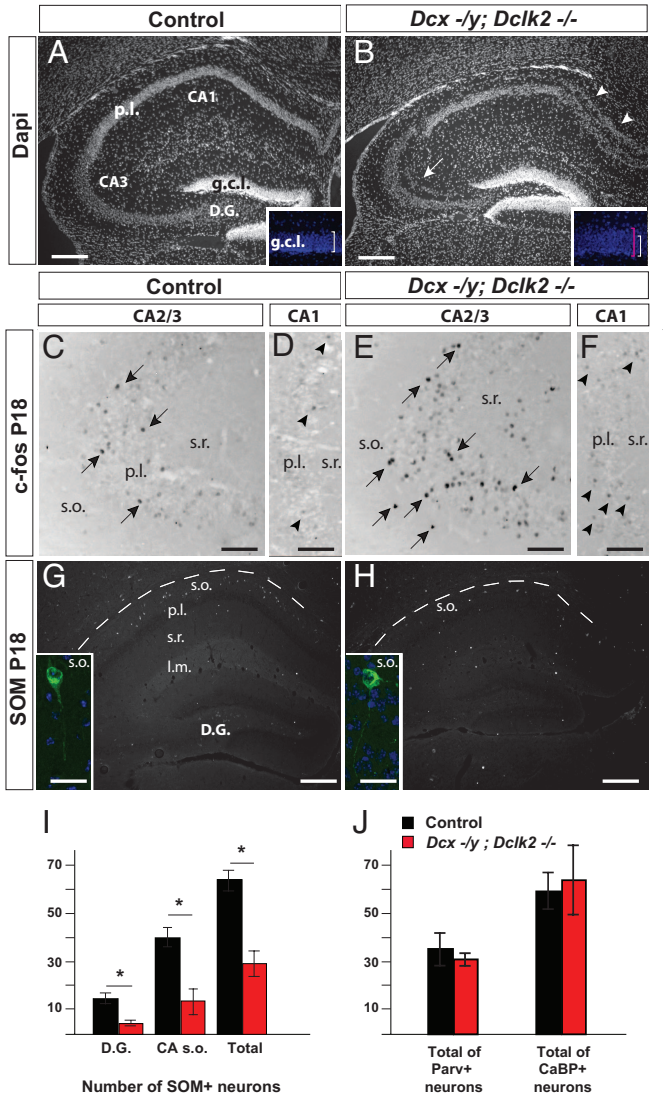

Fig. 2. Hippocampal disorganization, increased c-fos, and loss of SOM+ interneurons in *Dcx*; *Dclk2* nulls. (*A* and *B*) DAPI-stained P18 coronal hippocampus in control delineate densely packed GCL (g.c.l.) in the dentate gyrus (D.G.) and pyramidal layer (p.l.) in the CA field. In *Dcx*; *Dclk2* nulls the p.l. is delaminated in CA3 (arrow) and CA1 (arrowheads). The g.c.l. is also less packed and consequently thicker (*Insets*, compare brackets); $n = 4$. (*C–F*) *Dcx*; *Dclk2* null pyramidal neurons show higher levels and more c-fos-positive cells than controls in both CA2/3 (arrows in *C* and *E*) and CA1 (arrowheads in *D* and *F*) fields at P18; $n = 2$. (*G–J*) SOM+ interneurons in both the D.G. hilus and the strata oriens (s.o.) of the CA region. *Dcx*; *Dclk2* nulls show reduced number of SOM+ interneurons (30.44 ± 7.48 vs. 64.56 ± 6.74; $P = 0.0276$; $n = 3$ mice each), both in the D.G. (5.00 ± 0.51 vs. 16.22 ± 2.47; $P = 0.0113$), and in s.o. (15.89 ± 5.73 vs. 40.78 ± 4.64; $P = 0.0279$) (*H* and *I*). Remaining SOM+ interneurons express the same level of SOM (*Inset* in *G* and *H*). No significant difference in the total number of Parv+ (30.67 ± 1.67 in *Dcx*; *Dclk2* nulls vs. 36.33 ± 6.33 in controls; $n = 2$ mice of each genotype) or CaBP+ (63.15 ± 14.58 in *Dcx*; *Dclk2* nulls vs. 59.44 ± 7.99 in controls; $n = 3$ mice each); s.r., strata radiata; l.m., lacunosum moleculare. Dashed line delineates the hippocampal fissure. [Scale bars, 400 μm (*A*, *B*, *G*, and *H*); 110 μm (*C–F*).]

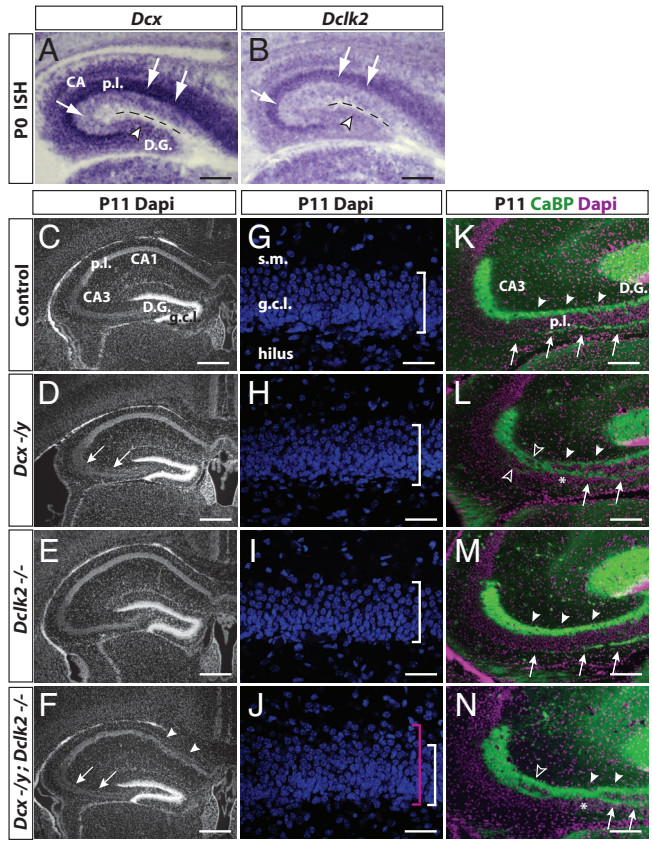

Fig. 3. *Dcx* and *Dclk2* expression and *Dcx*; *Dclk2* null hippocampal phenotype at earlier developmental stages. (*A* and *B*) In situ hybridization for *Dcx* and *Dclk2* at P0. *Dcx* and *Dclk2* are most highly expressed the CA region (arrows), D.G. (arrowheads), and in the nonprincipal cell layers. Dashed line delineates the dorsal limit of the D.G. (*C–J*) DAPI-stained P11 coronal hippocampal lamination in controls, single *Dcx* −/*y* and *Dclk2* −/−, and *Dcx*; *Dclk2* null mice. (*C–F*) Both *Dcx* −/*y* and *Dcx*; *Dclk2* nulls show delaminated pyramidal layer in CA3 (arrows), but only *Dcx*; *Dclk2* nulls show delaminated CA1 (arrowheads). *Dclk2* −/− morphology appears normal. (*G–J*) *Dcx*; *Dclk2* null granule layer is less packed and as a result thicker (brackets). (*K–N*) In control and *Dclk2* −/−, the IB (arrows) and SB (white arrowheads) surround the densely packed CA3 pyramidal layer proximal to the D.G. In *Dcx* −/*y* and *Dcx*; *Dck2* nulls the IB starts to form, but soon crosses massively the CA3 pyramidal layer (asterisks in *L* and *N*) to merge with the SB, which appears disrupted by groups of pyramidal cells (unfilled arrowheads); $n = 3$. [Scale bars, 140 μm (*A* and *B*); 400 μm (*C–F*); 25 μm (*G–J*); 200 μm (*K–N*).]

of major steps in hippocampal organization (P11). Nuclear staining in *Dcx*; *Dclk2* nulls at P11 demonstrated dyslamination of CA1 and CA3 identical to what was observed at P18 (Fig. 3 *C* and *F*), suggesting that this defect is not secondary to epilepsy. The *Dcx* −/*y* mice displayed dyslaminated CA3 field (Fig. 3*D*; see ref. 8), similar to *Dcx*; *Dclk2* nulls. However, *Dclk2* −/− hippocampus displayed normal lamination of the entire CA field (Fig. 3*E*). Together, the data suggest that *Dcx* deficiency is the major contributor to the lamination defect of the CA3 field, whereas *Dcx* and *Dclk2* have redundant roles in lamination of the CA1 field.

The GCL lamination density was normal in *Dcx* −/*y* and the *Dclk2* −/− compared with control mice (Fig. 3 *G–I*), but was increased in *Dcx*; *Dclk2* nulls (Fig. 3*J*), suggesting that *Dcx* and *Dclk2* are functionally redundant in regulating lamination/packing of the GCL. We next questioned whether this abnormal lamination/packing of GCL neurons might be associated with defects in axonal projections. The GCL projects CaBP+ mossy fibers to the apical and basolateral dendrites of CA3 pyramidal neurons along the suprapyramidal bundle (SB) and infrapyramidal bundle (IB), respectively. In *Dcx* −/− mice, the IB was evident in origin near the hilus, but cross the pyramidal layer to merge prematurely with the SB. In the *Dcx*; *Dclk2* nulls, this abnormality was even more apparent, with failure to separate the IB from the SB, and, as a result, fibers travel aberrantly within the pyramidal layer. In contrast, the IB formed normally in *Dclk2* −/− mice (Fig. 3 *K–N*). We conclude that the *Dcx* deficiency primarily drives the abnormal formation of the IB in the *Dcx*; *Dclk2*.

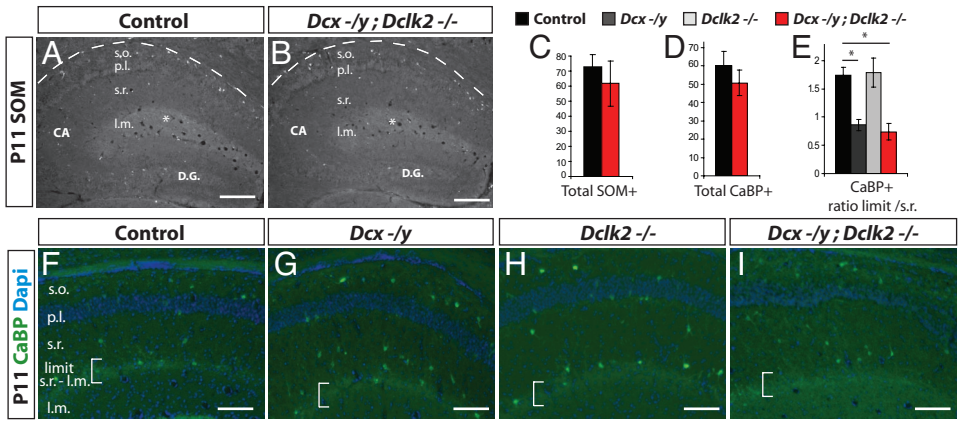

Fig. 4. Dyslaminated interneuron populations in *Dcx*; *Dclk2* nulls. (*A–C*) Total number of SOM+ interneurons is similar in control (*A* and *C*) (72.67 ± 8.50; $n = 3$ mice) and *Dcx*; *Dclk2* nulls (*B* and *C*) (61.71 ± 14.96; $n = 2$ mice). Level of SOM+ innervation by the O-LM cells to the l.m. is similar in the control and *Dcx*; *Dclk2* null hippocampus (asterisks in *A* and *B*). (*D–I*) Total number of CaBP+ interneurons is normal at this stage (*D*) (50.54 ± 6.97 in *Dcx*; *Dclk2* nulls vs. 60.10 ± 7.75 in controls; $n = 5$ controls, 3 nulls). However, the location of the CaBP+ interneurons within the CA field is abnormal in *Dcx* −/*y* and *Dcx*; *Dclk2* nulls. In control (*E* and *F*) and *Dclk2* −/− (*E* and *H*), the number of CaBP+ interneurons located at the limit between the s.r. and l.m. (limit, white bracket) is greater than the number of interneurons located within the rest of the s.r. (the ratio limit/s.r. are 1.73 ± 0.14 and 1.79 ± 0.25, respectively). This ratio is significantly lower in *Dcx* −/*y* (*E* and *G*) (0.86 ± 0.10; $P = 0.0152$ to control) or *Dcx*; *Dclk2* nulls (*E* and *I*) (0.74 ± 0.15; $P = 0.0103$ to control) hippocampus ($n = 5$ control, 2 of each single null and 3 double nulls). [Scale bars, 400 μm (*A* and *B*); 50 μm (*F–I*).]

Hippocampal Inhibitory Neuron Loss Follows the Onset of Epilepsy. We next tested whether the loss of SOM+ neurons that was observed after the onset of seizures was evident before the onset of seizures. At P11, there was no statistical difference in SOM+ neuron number between control and *Dcx*; *Dclk2* nulls (Fig. 4 *A–C*). Because the full complement of SOM+ neurons are already in place by this age (11), we conclude that the difference in numbers of SOM+ neurons detected at the later stage is due to secondary neuronal loss.

We evaluated lamination of CaBP+ interneurons, one of the major class that projects onto pyramidal neurons. Most of the CaBP+ interneuron somas (like a majority of the other GABAergic somas), redistribute postnatally to achieve final positions adjacent to the principal cell layers or in the stratum radiatum-lacunosum moleculare (s.r./l.m.) border. At P11, this lamination was disrupted in *Dcx* −/*y* and *Dcx*; *Dclk2* nulls, with failure of CaBP+ cells to laminate within the anatomically defined s.r./l.m. border (Fig. 4 *F–I*), despite a normal number of CaBP+ cells (Fig. 4 *D* and *E*). Noticeably, this defect was still observed at P18 (Fig. S4), suggesting that it is not just a temporary delay in maturation. Thus, *Dcx* deficiency appears to drive interneuron lamination, whereas *Dclk2* does not appear to make a major contribution to this effect.

GABA-Mediated Synaptic Inhibition Is Reduced in *Dcx*; *Dclk2* Null Pyramidal Neurons. We hypothesized that the overall disorganization of the inhibitory network might result in reduced inhibitory tone onto pyramidal neurons, contributing to the seizure onset. To test this possibility, we compared whole-cell inhibitory postsynaptic currents (IPSCs) from *Dcx*; *Dclk2* null and control littermates from CA1 neurons in acute slice preparations at P11–P14, before the onset of seizures. To avoid compounding effects of mispositioned pyramidal neurons, we focused our studies on correctly laminated pyramidal neurons. The frequency of spontaneous (s)IPSCs was severely reduced in the *Dcx*; *Dclk2* nulls compared with controls (overall reduction of 55%), suggesting reduced inhibitory tone. *Dclk2* −/− mice showed essentially normal sIPSCs frequency, whereas *Dcx* −/*y* mice showed an intermediate reduction of this frequency (Fig. 5 *A–C*). However, there was no alteration in the mean amplitude or amplitude distribution of the sIPSCs (Fig. 5 *D* and *E*), suggesting no alteration in synaptic strength for any genotype. The reduced inhibitory synaptic tone in the *Dcx*; *Dclk2* null pyramidal neurons and intermediate effects in the *Dcx* −/*y* are consistent with the overall graded network disorganization observed anatomically.

Pyramidal Neuron Apical Dendrite Branching Defect Suggests Reduced Receptive Fields. Because both *Dcx* and *Dclk2* encode microtubule-associated proteins, it is possible that they function together to regulate pyramidal neuron dendritic morphology to establish receptive field, which might account for the reduced sIPSC frequencies. Thus, we tested for defects in pyramidal CA1 neuron morphology by using Golgi–Cox staining at P11 (i.e., before seizures, to distinguish between dendrite shrinkage as a result of seizure). No morphological defects were detected in either the *Dcx* −/*y* or the *Dclk2* −/− neurons (Fig. 6 *B*, *C*, and *F*). In contrast, *Dcx*; *Dclk2* null pyramidal neurons displayed a striking simplification of apical dendritic arbors. There was a significant decrease in the number of

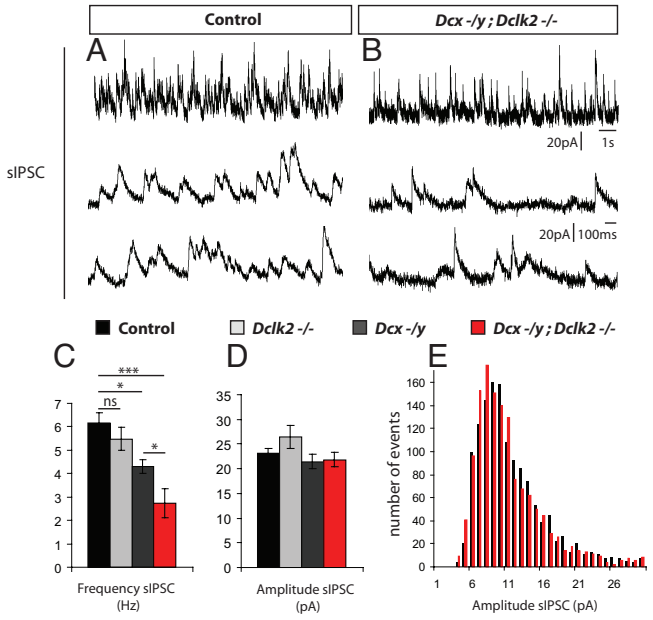

Fig. 5. GABAergic synaptic inhibition on pyramidal cells is reduced in frequency in *Dcx*; *Dclk2* nulls. (*A* and *B*) Representative traces of sIPSCs from CA1 pyramidal neurons of P11–P13 control (*A*) and *Dcx*; *Dclk2* nulls (*B*). (*C*) Average frequency of sIPSCs is significantly decreased in *Dcx*; *Dclk2* null (2.745 ± 0.6185; $n = 15$ neurons in $n = 3$ mice) cells compared with controls (6.1776 ± 0.4377; $n = 20$ neurons in $n = 4$ mice; $P < 0.001$). The frequency in *Dclk2* single null cells is unchanged (5.476 ± 0.4899; $n = 15$ neurons in $n = 3$ mice; $P > 0.05$). *Dcx* single null pyramidal cells show intermediate reduction of sIPSCs frequency (4.313 ± 0.2654, $n = 14$ neurons in $n = 3$ mice $P < 0.05$ compared with control, and $P < 0.05$ compared with *Dcx*; *Dclk2* nulls). (*D*) The average amplitude of sIPSCs is similar between controls (23.10 ± 0.950 pA), *Dclk2* nulls (26.41 ± 2.371), *Dcx* nulls (21.46 ± 1.443), or *Dcx*; *Dclk2* nulls (21.87 ± 1.536). (*E*) Amplitude distributions of sIPSCs is similar in *Dcx*; *Dclk2* null and control cells.

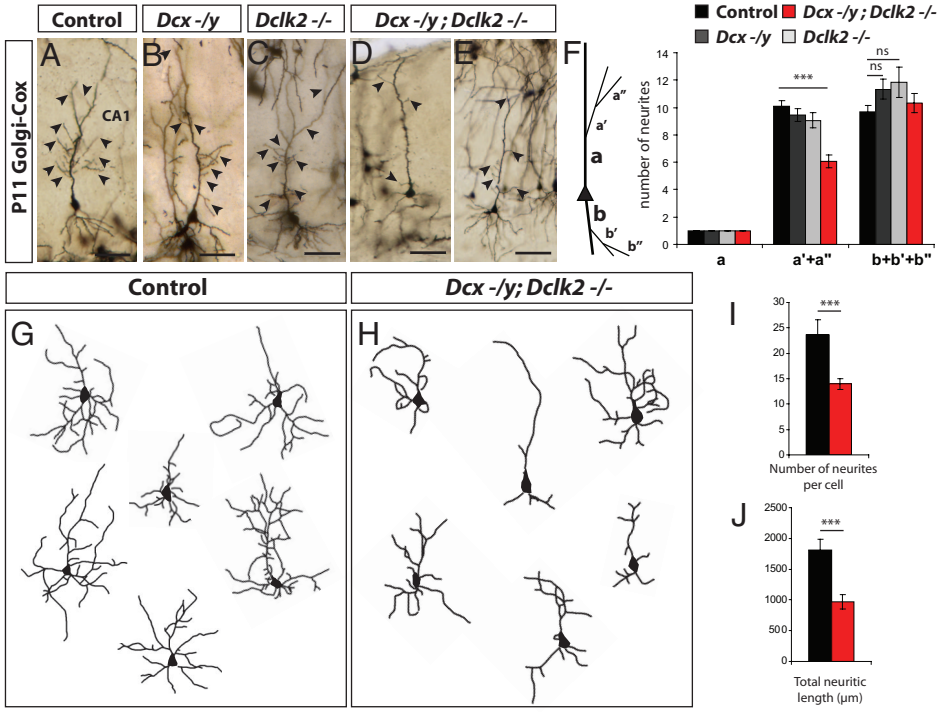

Fig. 6. Morphological defect of *Dcx*; *Dck2* null hippocampal pyramidal cells in vivo and in vitro. (*A–F*) Golgi–Cox-stained hippocampus at P11 showing *Dcx*; *Dclk2* nulls with less secondary and tertiary apical pyramidal dendrites (*D–F*) (6.06 ± 0.48; $n = 32$ neurons, $n = 2$ mice) than controls (*A* and *F*) (10.09 ± 0.39; $n = 53$ neurons in $n = 3$ mice; $P < 0.001$). Dendrite number in *Dcx* (*B* and *F*) (9.46 ± 0.48 $n = 40$ neurons in $n = 2$ mice) or *Dclk2* (9.06 ± 0.57; $n = 35$ neurons in $n = 2$ mice) single knockouts is normal. Total number of basolateral dendrites is normal in all (*F*) (10.33 ± 0.69 in *Dcx*; *Dclk2* nulls, 11.53 ± 0.73 in *Dcx* nulls, 11.88 ± 1.12 in *Dclk2* nulls vs. 9.71 ± 0.48 in controls; $n = 32–53$ neurons, $n = 3$ control mice and $n = 2$ mice each). (*G–J*) Neurite outgrowth of *Dcx*; *Dclk2* null pyramidal cells is greatly reduced compared with controls. Both the total number of neurites (*I*) (13.95 ± 1.08 in *Dcx*; *Dclk2* nulls vs. 23.67 ± 2.92 in control; $P = 0.0006$; $n = 21$ and 9 neurons) and total length of neurites (*J*) (967.56 ± 119.12 in *Dcx*; *Dclk2* nulls vs. 1809.44 ± 179.02 in control; $P = 0.0006$; $n = 21$ and 9 neurons; $n = 2$ mice each) are significantly reduced. [Scale bars, 40 μm (*A–E*).]

dendrites branching from the primary (a) and secondary (a′) apical dendrites (Fig. 6 *A* and *D–F*). There were no notable differences in the size of the soma, the length of the primary apical dendrite, the length or branching of basolateral dendrites, or in their orientation with respect to the pial surface. Also, observation of dendritic spines at high magnification revealed no obvious abnormality in morphology or density (Fig. S5 *A–F*). GCL neurons showed no obvious morphological abnormalities in dendritic morphology, branching, or complexity (Fig. S3*B*), suggesting a specific effect of *Dcx* and *Dclk2* mutations on dendrite morphology in large complex pyramidal neurons.

We questioned whether the in vivo defect in pyramidal neuron branching complexity was cell autonomous or due to altered lamination. Therefore, we cultured hippocampal neurons from mice at P0 from wild-type and *Dcx*; *Dclk2* nulls (genotypes where the dendritic differences were detected in vivo) and observed after 16 days in vitro (DIV). Before fixation, cells were infected with low-titer EGFP-expressing virus to precisely delineate morphology. Only cells showing pyramidal morphology and absence of GABA staining (i.e., excitatory neurons) were included for quantification. The number of branch points and the total length of dendrites were reduced in *Dcx*; *Dclk2* nulls compared with controls (Fig. 6 *G–J*). We conclude that *Dcx* and *Dclk2* are together required for development of dendritic branching complexity and growth in hippocampal pyramidal neurons independently from altered neuron positioning.

Discussion

Here, we demonstrate that DCX and DCLK2 share function in the establishment of hippocampal organization and that their absence results in a severe epileptic phenotype and lethality, as described in human patients with lissencephaly. The *Dcx*; *Dclk2* nulls show an overall disorganized hippocampal network with mispositioned excitatory and inhibitory neurons, and defective circuitry, leading to reduced inhibitory tone onto pyramidal neurons. Also, the *Dcx*; *Dclk2* null pyramidal neurons show altered apical dendritic morphology. These 2 effects were correlated with excessive excitability of pyramidal neurons and subsequent epileptic seizures. These seizures temporally led to a secondary loss of the SOM+ class of inhibitory interneurons, further altering the balance of excitation and inhibition. The DCX family members are key regulators of the neuronal cytoskeleton (12), which is critical for migration and establishment of neuronal morphology. We hypothesize that cytoskeletal alterations contribute to the epileptogenic transformation of the hippocampus in the *Dcx*; *Dclk2* null mouse (Fig. S6). *Dcx*; *Dclk2* nulls constitute a model of X-linked lissencephaly displaying both epilepsy and associated lethality, and they could be used to help evaluate possible future therapies.

Network Disruption in Models of Hippocampal Epilepsy. It is interesting that the timing of the seizures in the *Dcx*; *Dclk2* nulls corresponds approximately to the onset of seizures in human lissencephaly. Patients with lissencephaly usually display seizures at ≈3 months, which approximately corresponds with postnatal days 7–14 in rodents. Surprisingly, in this model, the seizures do not emanate from the neocortex, but from the hippocampus, a finding with relevance to human generalized disorders of neuronal migration. For example, some individuals with these generalized disorders of neuronal migration have been found to have hippocampal onset seizures, and resections of these areas of epileptogenesis have demonstrated mixed results (13, 14).

Spontaneous seizures have been reported in some but not all animals with hippocampal or cortical dysgenesis. Lethal tonic–clonic seizures were occasionally observed in the *Pafah1b1* (platelet-activating factor acetylhydrolase 1B α subunit, encoding LIS1), but not reported in α1-tubulin mutant mice, both of which lead to a classical lissencephaly phenotype in humans when mutated (15, 16). *Pafah1b1* mice showed stunted basal dendrites of heterotopic CA1, but not in normally positioned pyramidal neurons (17), suggesting that, in this model, the dendritic abnormalities are secondary to mispositioning. Also, in these mice, hippocampal interneurons showed altered positioning and an increased spontaneous firing (17, 18), resulting in an increased pyramidal neuron IPSCs frequency (16). Thus, *Pafah1b1* mutants probably represent different seizure pathogenesis from *Dcx*; *Dclk2* nulls or other epilepsy models showing a decrease of IPSC frequency. The *p35* (*cdk5r1*) nulls display severe dyslamination of pyramidal and granule cell neurons that

contribute to seizure activity by forming an abnormal excitatory feedback circuit (19). Thus, the mechanisms underlying epilepsy are gene-specific, but point to the importance of lamination and dendritic maturation in hippocampal development.

Dendritic Branching and Neuronal Excitation. Abnormalities of dendritic morphology are common in cortical neurons of human partial epilepsy (20). Also, both neuronal modeling and experimental studies have demonstrated that alterations of dendritic morphology can significantly affect neuronal excitability (21, 22). We found that the alteration of pyramidal neuron dendritic branching is correlated with reduced inhibition, which precedes the loss of SOM+ neurons and the development of overt seizures. The data suggest that this impaired maturation, through a reduction in receptive field, leads to insufficient inhibitory input, which tips the excitation–inhibition balance. We found normal pyramidal neuron postsynaptic dendritic spine morphology (Fig. S5 *A–F*), and normal density of glutamic acid decarboxylase (GAD65/67) presynaptic boutons on the perisomal region of pyramidal neurons (one of the major sites of inhibition, see Fig. S5 *G* and *H*), suggesting that inhibitory synapses can form normally on the remaining receptive field. However, the lacunosum moleculare is one of the other major sites of inhibitory input, and we observed a dramatic reduction in dendritic branching along the whole apical dendrite, including in this layer; thus, it is likely the explanation for the reduced inhibitory inputs.

Because apical dendrites receive both inhibitory and excitatory inputs, why might a reduction in branching lead to excessive hippocampal activity? The physical location of excitatory vs. inhibitory input synapses, receptor density, and channel density all affect the integration of the signal and are probably critical in determining the response pattern of an individual neuron. Therefore, aberrant morphology might cause defective integration of the excitatory and inhibitory inputs and modify their relative contribution. Balancing excitation and inhibition is critical for generating regulated output from the hippocampus, and refinement of the morphology is probably under strict homeostatic control to maintain this balance (23), which may be lost in the *Dcx*; *Dclk2* null pyramidal neurons.

Addendum. Nosten-Bertrand et al. (24) recently published that *Dcx* single nulls can develop rare seizures. A potential explanation for this discrepancy is the use of the C57BL/6N (B6) background by Nosten-Bertrand et al. (24), which is associated with a lowered seizure threshold in some mutant mice (25), whereas we used a mixed 129/SvJ and B6 background.

Materials and Methods

***Dclk2* Targeting.** The targeting of the constitutive exon 2 was performed by using published methods, with removal of the conditional cassette by using EIIa-Cre (4).

EEG Electrode Implantation, Video Monitoring, and Analysis. Hippocampal and cortical recordings were performed in freely moving, nonanesthetized mice as reported (26). Seizure characteristics retained for analysis are presented in *SI Materials and Methods*.

Histochemistry. In situ hybridization and immunochemistry information and antibody references are presented in *SI Materials and Methods*. Golgi–Cox staining was performed as recommended (FD Neurotechnologies).

Neuron Quantification. Detailed methodology for neuron quantification and dentate GCL volume calculation are presented in *SI Materials and Methods*.

Dissociated Hippocampus Neuron Culture. Culture protocols and analysis methodology are presented in *SI Materials and Methods*. EGFP was cloned into SinRep5 (Invitrogen) and used as recommended. Titer was adjusted to 1% cell infection.

Electrophysiology. Brains were sectioned as described in ref. 27. IPSPs were recorded as described in ref. 7 with the following exceptions. Intracellular patch solution contained (in mM): 140 cesium gluconate, 8 NaCl, 5 EGTA, 1 QX-314, 2 MgATP, 0.3 LiGTP, 10 Hepes, pH 7.25 (280 mOsm). Values per cell are mean ± SEM of 100 IPSCs. Genotypes were compared by using unpaired 2-tailed *t* tests.

ACKNOWLEDGMENTS. We thank Orly Reiner (Weizmann Institute of Science, Rehovot, Israel) for the *Dclk2* in situ probe, Arthur Edelman (State University of New York, Buffalo) for the Dclk2 affinity-purified antibody, and Massimo Scanziani (University of California, San Diego) for helpful suggestions and critical reading of the manuscript. This work was supported by University of California at San Diego, Neurosciences Microscopy Imaging Core (P30 NS047101), the Electrophysiology Core of the La Jolla Interdisciplinary Neuroscience Center Core (Principal Investigator Stuart Lipton), and by grants from the National Institutes of Health, the Burroughs Wellcome Fund, and the Howard Hughes Medical Institute. G.K. is supported by a European Molecular Biology Organization fellowship, and H.K. by the Epilepsy Foundation and the National Institutes of Health.

1. Porter BE, et al. (2003) Dysplasia: A common finding in intractable pediatric temporal lobe epilepsy. *Neurology* 61:365–368.
2. Kerjan G, Gleeson JG (2007) Genetic mechanisms underlying abnormal neuronal migration in classical lissencephaly. *Trends Genet* 23:623–630.
3. Brown JP, et al. (2003) Transient expression of doublecortin during adult neurogenesis. *J Comp Neurol* 467:1–10.
4. Koizumi H, et al. (2006) Doublecortin-like kinase functions with doublecortin to mediate fiber tract decussation and neuronal migration. *Neuron* 49:55–66.
5. Deuel TA, et al. (2006) Genetic interactions between doublecortin and doublecortin-like kinase in neuronal migration and axon outgrowth. *Neuron* 49:41–53.
6. Edelman AM, et al. (2005) Doublecortin kinase-2, a novel doublecortin-related protein kinase associated with terminal segments of axons and dendrites. *J Biol Chem* 280:8531–8543.
7. Cobos I, et al. (2005) Mice lacking Dlx1 show subtype-specific loss of interneurons, reduced inhibition and epilepsy. *Nat Neurosci* 8:1059–1068.
8. Kappeler C, et al. (2007) Magnetic resonance imaging and histological studies of corpus callosal and hippocampal abnormalities linked to doublecortin deficiency. *J Comp Neurol* 500:239–254.
9. Morgan JI, et al. (1987) Mapping patterns of c-fos expression in the central nervous system after seizure. *Science* 237:192–197.
10. Sun C, et al. (2007) Selective loss of dentate hilar interneurons contributes to reduced synaptic inhibition of granule cells in an electrical stimulation-based animal model of temporal lobe epilepsy. *J Comp Neurol* 500:876–893.
11. Danglot L, et al. (2006) The development of hippocampal interneurons in rodents. *Hippocampus* 16:1032–1060.
12. Coquelle FM, et al. (2006) Common and divergent roles for members of the mouse DCX superfamily. *Cell Cycle* 5:976–983.
13. Tai PC, et al. (2004) Surgical resection for intractable epilepsy in ''double cortex'' syndrome can yield adequate results. *Epilepsia* 45:562–563.
14. Bernasconi A, et al. (2001) Surgical resection for intractable epilepsy in ''double cortex'' syndrome yields inadequate results. *Epilepsia* 42:1124–1129.
15. Keays DA, et al. (2007) Mutations in alpha-tubulin cause abnormal neuronal migration in mice and lissencephaly in humans. *Cell* 128:45–57.
16. Jones DL, Baraban SC (2007) Characterization of inhibitory circuits in the malformed hippocampus of Lis1 mutant mice. *J Neurophysiol* 98:2737–2746.
17. Fleck MW, et al. (2000) Hippocampal abnormalities and enhanced excitability in a murine model of human lissencephaly. *J Neurosci* 20:2439–2450.
18. Nasrallah IM, et al. (2006) Analysis of non-radial interneuron migration dynamics and its disruption in Lis1+/− mice. *J Comp Neurol* 496:847–858.
19. Patel LS, et al. (2004) Physiological and morphological characterization of dentate granule cells in the p35 knock-out mouse hippocampus: Evidence for an epileptic circuit. *J Neurosci* 24:9005–9014.
20. Belichenko PV, et al. (1994) Dendritic morphology in epileptogenic cortex from TRPE patients, revealed by intracellular Lucifer Yellow microinjection and confocal laser scanning microscopy. *Epilepsy Res* 18:233–247.
21. Gunnersen JM, et al. (2007) Sez-6 proteins affect dendritic arborization patterns and excitability of cortical pyramidal neurons. *Neuron* 56:621–639.
22. Mainen ZF, Sejnowski TJ (1996) Influence of dendritic structure on firing pattern in model neocortical neurons. *Nature* 382:363–366.
23. Samsonovich AV, Ascoli GA (2006) Morphological homeostasis in cortical dendrites. *Proc Natl Acad Sci USA* 103:1569–1574.
24. Nosten-Bertrand M, et al. (2008) Epilepsy in Dcx knockout mice associated with discrete lamination defects and enhanced excitability in the hippocampus. *PLoS ONE* 3:e2473.
25. Yu FH, et al. (2006) Reduced sodium current in GABAergic interneurons in a mouse model of severe myoclonic epilepsy in infancy. *Nat Neurosci* 9:1142–1149.
26. Dube C, et al. (2006) Temporal lobe epilepsy after experimental prolonged febrile seizures: Prospective analysis. *Brain* 129:911–922.
27. Saganich MJ, et al. (2006) Deficits in synaptic transmission and learning in amyloid precursor protein (APP) transgenic mice require C-terminal cleavage of APP. *J Neurosci* 26:13428–13436.